Surface Recognition via Force-Sensory Walking-Pattern Classification for Biped Robot

Aiwen Luo, *Member, IEEE*, Sandip Bhattacharya, Sunandan Dutta, Yoshihiro Ochi, Mitiko Miura-Mattausch, *Fellow, IEEE*, Jian Weng, *Member, IEEE*, Yicong Zhou, *Senior Member, IEEE*, and Hans J. Mattausch, *Senior Member, IEEE*

***Abstract*—Real-time surface recognition has become a critical factor for ensuring safe walking of intelligent biped robots in a complex human living environment. This work aims at enabling wide cost-efficient implementation of sensing solutions for surface recognition via walking-pattern classification by restricting the necessary hardware to a cost-economic microprocessor and a single type of force sensors. For experimental analysis, we explored the walking-pattern classification performance using a framework which combines a support vector machine (SVM) and four time-domain feature descriptors, i.e., mean of amplitude (MA), integral of absolute value (IAV), variance (VAR), and root mean square (RMS). During the online pattern classification, the dynamical force-sensory-data stream was extracted using a real-time overlapped-window-based method. Multiple binary SVM classifiers were applied for solving the multi-class classification problem, due to the reasonably high accuracy and the relatively small complexity for hardware implementation, allowing simultaneous strength exploitation of above four individual feature descriptors with a one-versus-one (OVO) strategy. The experimental results, obtained with 250 samples/surface, verified 93.8% mean average precision, 93.7% average accuracy and recall rates of 98.8%, 91.6%, 82.0%, 98.0%, 98.0% for smooth wood, rough foam, smooth foam, thick carpet, and thin carpet, respectively. Only the dynamical force-sensing data were employed for a 10-fold cross validation, which enabled the high processing speed of 0.73 ms/stride. The developed cost-efficient and accurate surface-recognition system can be useful for ensuring safe in-door locomotion for the biped robot and can help the robot to better understand the human living environment by increasing its sensing diversity.**

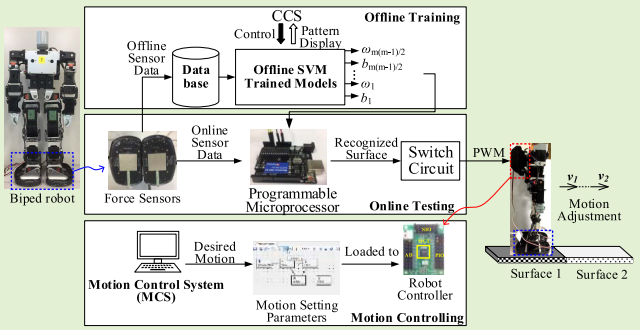

***Index Terms*—Biped robot, force sensor, multi-class SVM, surface recognition, walking-pattern classification.**

Manuscript received January 14, 2021; accepted February 9, 2021. Date of publication February 12, 2021; date of current version March 17, 2021. This work was supported in part by the TAOYAKA Program for Creating a Flexible, Enduring, and Peaceful Society, Hiroshima University, supported by the NSFC, under Project 62002134, in part by the Fundamental Research Funds for the Central Universities at Jinan University under Grant 21620353, in part by the Science and Technology Development Fund, Macau SAR, under Grant 189/2017/A3, and in part by the University of Macau under Grant MYRG2018-00136-FST. The associate editor coordinating the review of this article and approving it for publication was Prof. Yudong Zhang. *(Corresponding author: Aiwen Luo.)*

Aiwen Luo is with the College of Information Science and Technology, Jinan University, Guangzhou 510632, China, also with the Department of Computer and Information Science, University of Macau, Macau 999078, China, and also with the HiSIM Research Center, Hiroshima University, Higashihiroshima 739-8530, Japan (e-mail: faith.awluo@gmail.com).

Sandip Bhattacharya, Sunandan Dutta, Yoshihiro Ochi, Mitiko Miura-Mattausch, and Hans J. Mattausch are with the HiSIM Research Center, Hiroshima University, Higashihiroshima 739-8530, Japan (e-mail: hjm@hiroshima-u.ac.jp).

Jian Weng is with the College of Information Science and Technology, Jinan University, Guangzhou 510632, China (e-mail: cryptjweng@gmail.com).

Yicong Zhou is with the Department of Computer and Information Science, University of Macau, Macau 999078, China (e-mail: yicongzhou@um.edu.mo).

Digital Object Identifier 10.1109/JSEN.2021.3059099

I. Introduction

ROBOT systems are fostered by intelligent techniques throughout the years and are very soon expected to assist and support humans in lots of potential applications. Safe locomotion on different surfaces in an unknown environment is considered as one of the major challenges for robots. With the increasing trend towards home service and medical treatment [1], biped robots with walking capabilities like humans have gained much attention. Recognition techniques for identifying various unknown terrains or underlying surfaces turn out to be essential for improving the navigation ability of robots [2].

A. Related Works

To maintain the stability during walking for biped robots, many studies have proposed methods which are based on an understanding of the human learning mechanisms, like push recovery strategies [3], [4] or joint trajectory combinations [5], [6]. Multifarious recognition approaches have been developed as well for various robots over the

last decades, being based on diverse types of sensors and combinations of sensors.

Sensor types can be divided into two main categories, i.e., contact sensors and non-contact sensors. Non-contact sensing solutions are programmed to mimic human senses and use mostly visual, acoustical, or optical sensors for terrain/surface classification. Robotic vision can be a direct and effective way to perceive the environment changes during locomotion as reported in [7], [8]. However, the vision-based recognition solutions usually tend to be susceptible to luminance changes, while having additionally high computational cost and comparatively low processing speed. Acoustics-based solutions [9], [10] classify the terrains by listening to the sounds generated during robot locomotion. Unfortunately, classification performance is to a great extent susceptible to background noise. Optical sensors such as lasers [11] may turn out to be ineffective for correct perception of the environment, when the laser beam is blocked because the receiver cannot always be maintained properly. More significantly, the surface properties can be hardly perceived by the non-contact sensing solutions due to the missing physical interactions between the robot and the ground surface.

The actual contact information through the physical interaction is of considerable significance for understanding environments, so as to select an appropriate mode of motion for the robot. Thus, numerous contact-sensor-based schemes are investigated by relying on direct contact information of the ground properties through application of different tactile sensors such as inertial measurement unit (IMU) or force/torque (F/T) sensor. DuPont *et al.* [12] proposed an autonomous classification algorithm for wheeled vehicles using measured IMU data and obtained a classification accuracy $>70\%$ by applying a probabilistic neural network (PNN) classifier. An accelerometer-based intelligent tire [13] was developed for wheeled ground robots to use measured acceleration signals for terrain classification based on a fuzzy-logic algorithm. Similar previous approaches [14]–[16] use IMUs equipped with axis accelerometer sensors for surface identification through measurement of the body vibration.

In comparison to the mobile robots such as wheeled robots and tracked robots [17], legged robots can operate in a much greater scope of surface diversities due to the high number of degrees of freedom (DoF). In other words, legged robots are more flexible for traversing various obstacles demanding greater control complexity. Shill *et al.* [18] used a one-legged hopping robot equipped with a pressure-sensing array to generate pressure images through direct surface contact, which enabled similarly textured surfaces to be distinguished with $\approx$99% identification accuracy. Ho *et al.* [19] designed a fabric sensor as the robot's skin that was applied for surface identification using discrete wavelet transform (DWT) and artificial neural network (ANN). Wu *et al.* [20] applied capacitive tactile sensors at the feet of a small hexapod robot for measuring the contact forces and identified terrain types using the support vector machine (SVM) with 82.5% accuracy. Multiple sensors can be combined to obtain better surface recognition performance [21]. Extensive surface-classification studies, using different sensors and classifiers, were performed with various legged robots such as hexapod robots [20]–[22], quadruped robots [23]–[26], and biped robots [27]–[29].

Safe locomotion is an essential requirement for the biped robots, since they are more likely to fall, even when walking on a flat surface, when compared to other legged robots. Matsumura *et al.* calculated mean and standard deviation of each inertial-sensor data, extracted from the full body of a small humanoid robot as features, constructed the classifier by decision trees [27] and achieved 85.7% precision. The fourth-order moment of the ground reaction force was determined as a feature for detecting unexpected large disturbances before mapping them to a logistic regression model for biped robots in [28]. Raw data from force sensors, installed on the humanoid robot NAO, were separated and normalized as inputs for two intelligent classifiers, i.e., ANN and extreme learning machine (ELM), resulting in $\approx$99% accuracy in [29]. The data from the F/T sensors, mounted on a humanoid robot's ankles, were further reduced by fast Fourier transform (FFT) and DWT, before transmission to the performed learning procedure using SVM, achieving precisions of about 95% and 91%, respectively, in [30]. Classifiers based on deep neural networks (DNNs) have been shown to have superior surface-classification performance when compared with the SVM model. But the DNNs-based approaches require large datasets for training and large computing resources for online recognition, which may not be feasible in practical robotic applications. A more complex solution, combining CNN with SVM, was reported in [31] for tactile-object recognition with higher recognition accuracy.

Inspired by the previous works on surface recognition and the enormous potential of biped robots for indoor applications in human-populated environments, such as hospitals, offices, and homes, we focus on developing intelligent and cost-economic surface-recognition designs for biped robots. We have previously reported a surface-property recognition scheme for stable humanoid-robot walking by using the k-nearest-neighbor (kNN) classifier in [32] and evaluated the influence of the walking speed on the recognition accuracy in [33]. The kNN classifier was found to require more computing resources, such as memory space for storing sufficient reference samples, for achieving higher classification accuracy.

B. Contributions

An online multi-class SVM classification solution was applied for high-accuracy and hardware-efficient dynamic recognition of robot-walking characteristics, employing cost-economic, ultra-thin, and velocity-sensitive membrane force sensors [38]. Specifically, the contributions and novelties of this research work lie in

- applying four computing-efficient time-domain features and their combination to reduce interferential noise of force sensor data, while using an overlapped-window-based method for real-time walking surface recognition;
- developing a resource-efficient and accurate multi-class SVM algorithm, based on physical interactions between indoor surfaces and the robot feet, for reducing resource consumption and computing time;

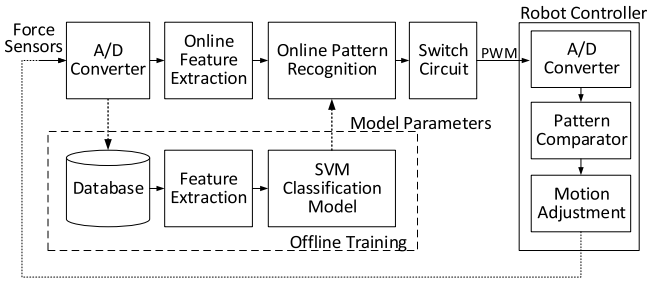

Fig. 1. Overall framework of dynamic walking-pattern recognition for surface identification by biped robots based on force sensors.

- implementing economic hardware-oriented classification based on the low-cost Arduino UNO board.

Consequently, this work proposes a hardware-oriented classification approach, implemented with a resource-efficient multi-class SVM algorithm, which reduces resource consumption and computing time, while leading to improved classification accuracy and fast recognition speed in the multi-class problem of detecting multiple surfaces for a biped robot in real time. From a practical point of view, hardware-oriented implementation can be considered as crucial for enabling a fast and accurate recognition model in general low-cost biped-robot applications with limited resources.

The paper organization is as follows. Section II describes the methodology of feature extraction and multi-class classification used for our force-sensory walking-pattern recognition. Section III describes the system development for surface-properties recognition. In Section IV, experimental setups and results are presented and discussed. This paper concludes in Section V and our plan for future work is exhibited in Section VI.

II. Recognition Methodology

A. Overall Recognition Framework

We propose the method shown in Fig. 1 to identify the flat floor surface on which a biped robot is walking, by sensing the physical interactions between the floor surface and the robot feet, using cost-economic force sensors. The core constructs of the surface-recognition methodology lie in the two phases of feature extraction and walking-pattern classification.

Considering the lower complexity for implementation on a microprocessor with limited hardware resources and the comparable recognition accuracy, a modified multi-class SVM approach with linear kernel is proposed for recognition of multiple indoor surfaces by the biped robot. Four computing-efficient feature descriptors were estimated individually with the multi-class SVM and were further allied together for getting higher classification accuracy.

B. Feature Extraction of Force-Sensory Information

The precise ground-contact forces normally include lots of interferential noise, making the raw force-sensory information improper for direct use in the surface-recognition task. A proper feature descriptor can grasp the core information, reduce computational cost and noise interference, and improve the classification accuracy. Thus, feature extraction becomes an extremely important part of the surface recognition.

Time-domain features are the most popular in classification tasks, due to their comparatively efficient computing properties. Inspired by the feature description for vibration signals like electromyography (EMG) signals [34], [35], we have investigated the impacts of the following four most-widely used descriptors on the recognition performance, when using time-domain force-sensory data.

1) Root Mean Square (RMS): RMS measures the amplitude of force sensory data, which is similar to the standard deviation calculation as well. Its mathematical expression is defined as

$$v_{RMS}(n) = \sqrt{\frac{1}{N}\sum_{k=1}^{N} x_k^2(n)}. \tag{1}$$

2) Integral of Absolute Value (IAV): The IAV feature is more commonly known as the mean absolute value (MAV) [36]. The MAV value of the force-sensory signal within an analysis window is estimated according to

$$v_{IAV}(n) = \frac{1}{N}\sum_{k=1}^{N} |x_k(n)|. \tag{2}$$

3) Variance (VAR): The variance measures the average power of the force-sensory signal according to

$$v_{VAR}(n) = \frac{1}{N-1}\sum_{k=1}^{N} x_k^2(n). \tag{3}$$

4) Mean of Amplitude (MA): MA has also been named wave length (WL) [36] as it estimates the waveform complexity in each length interval of two consecutive sensor-data points according to

$$v_{MA}(n) = \sum_{k=1}^{N-1} |x_{k+1}(n) - x_k(n)|. \tag{4}$$

Here, n is a time index in (1) to (4) for dynamic feature extraction from N sensor-data points of the force sensors.

C. Classification Strategy for Multi-Class SVM

To estimate the performance of the surface recognition, we employed the SVM classifier with a linear kernel, because of its high classification accuracy as well as its high computational efficiency, leading to economical hardware-resource requirements. A new surface type for observation can be easily assigned to one labeled category in the testing phase, based on a comparatively small number of trained model parameters.

The standard SVM was originally designed for binary classification tasks, separating data to one or the other of two categories by the hyperplane which can be expressed as

$$f_{SVM}(v) = \omega^T \cdot \varphi(v) + b, \tag{5}$$

where the column vector $\omega = (\omega[1]; \omega[2]; \ldots; \omega[d])$ refers to a d-dimensional weight vector that is normal to the separating hyperplane, b is a scalar bias, and $\varphi(v)$ is the kernel function for mapping the original feature space to another space for solving various classification problems. Kernel functions such as Gaussian basis function or polynomials can be applied for non-linearly separable classes. Nevertheless, the SVM classifier with a linear kernel, that uses its original feature space with a self-mapping function φ: $\varphi(v) \rightarrow v$, is employed in this work to improve hardware efficiency. The row vector $v = (v[1], v[2], \ldots, v[d])$ is the dynamical feature vector.

Since the original standard SVMs do not support multi-class classification natively, meta-strategies are required for solving a multi-class problem. Two typical extension approaches from the binary SVM classifier are: one-versus-one (OVO) and one-versus-rest (OVR). The OVR approach constructs m binary SVM models, where m is the number of classes. Each binary SVM model is sequentially trained by marking one class with a positive label and the remaining classes with a negative label. The OVR approach chooses the class which classifies the new observation sample with the greatest margin to the hyperplane according to

$$class_{OVR} \equiv \arg\max(\omega_i^T \cdot \varphi(v) + b_i), \quad i = 1, \ldots, m. \tag{6}$$

By contrast, the OVO strategy builds $m(m-1)/2$ binary SVM classifiers, splitting a m-class classification task into a set of binary-classification tasks for each pair (i, j) of combined classes, to solve the quadratic optimization problem:

$$\min_{\omega_{ij}, b_{ij}, \xi_{ij}} \quad \frac{1}{2}\omega_{ij}^T \omega_{ij} + C \sum_k \xi_{ij}(k),$$
$$s.t. \quad y_k \left(\omega_{ij}^T \cdot \varphi(v(k)) + b_{ij}\right) \geq 1 - \xi_{ij}(k), \quad \xi_{ij}(k) \geq 0. \tag{7}$$

Here, a vector of labels $\boldsymbol{y} \in R^m$, such that $\boldsymbol{y}_k \in \{+1, -1\}$ is the class of the $\varphi(v(k))$, where k = 1, …, m. C is a penalty parameter and ξ_{ij}(k) is a slack variable for reducing the training errors. The OVO strategy predicts the class of the test data by using the voting strategy of "max-wins", which chooses the class with the highest vote number from all binary classifiers.

In comparison, the OVR approach needs to construct fewer binary SVM models than the OVO method, but the OVR method is not a very elegant approach for solving multi-class problems, since it usually leads to an imbalanced binary classification where the number of positive samples normally differs tremendously from the number of negative samples. The time consumption for training classifiers in the OVO approach may on the other hand decrease significantly, since the training dataset for each binary classifier is much smaller.

III. System Development

We developed a robust and cost-effective system for surface recognition shown in Fig. 2, which measures the real-time physical interactions between the different surfaces and the robot feet by force sensing. The developed system enables a safe walking of a biped robot with an appropriate motion through an adaptive feedback control. The system is based on acquiring knowledge about the present surface type by recognizing the vibration signals from the force sensors mounted beneath the two feet of the biped robot.

A. Robot Platform

In our experiments we use the Kondo KHR-3HV humanoid robot [37], which is mainly constructed by 17 servomotors and a robot controller implemented on an RCB-4HV board, as illustrated in Fig. 3. The desired robot motion is designed in advance by a specific software tool installed on a master

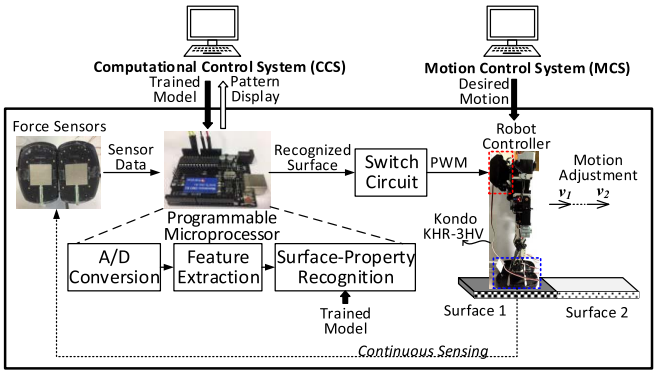

Fig. 2. Diagram of overall system for dynamic motion adjustment for the biped robot, based on surface-property recognition using force sensors.

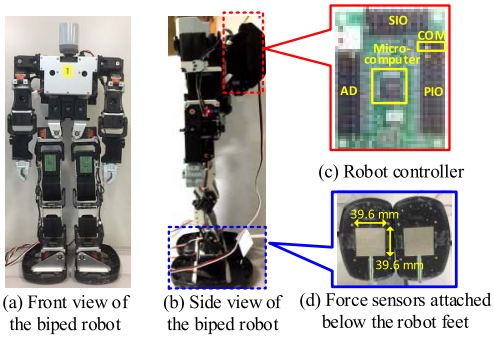

(a) Front view of the biped robot (b) Side view of the biped robot (c) Robot controller (d) Force sensors attached below the robot feet

Fig. 3. Hardware of the biped-robot platform, equipped with the robot controller (c) and two force sensors (d) for dynamical surface recognition, using the Kondo KHR-3HV robot shown in front view (a) and side view (b).

computer, i.e., the Motion Control System (MCS). The setting parameters of the complete robot motion are then loaded onto the microcomputer of the robot controller through a COM port at a maximum communication speed of 1.25 Mbps.

B. Sensor and Data Preprocessing

Cost-economic, ultra-thin, and velocity-sensitive membrane force sensors [38] are attached beneath each foot of the biped robot for measuring the real-time physical interactions between the underlying surface and the robot feet. The active area of 39.6 mm^2 of the force sensor responds to an increase in force during robot movement, due to inertia and gravity effects. The force-sensory signals are converted by the force sensors to vibrational voltage signals in the range of [0V, 5V], that act as system inputs. Preprocessing steps are necessary to achieve faster digital data computing. As analog signals, the equivalent vibrational voltages are sampled at a desired sampling rate and converted by an analog-to-digital conversion to serial discrete voltage points, which are described as 10-bit digital data, according to the equation: Vout_sensor(i) = 5*Dforce(i)/1024. Here Vout_sensor(i) refers to output voltages transmitted from the force sensors, and Dforce(i) represents the integer values between 0 and 1023 after AD conversion. We employed an Arduino UNO board as the programmable microprocessor for data pre-processing, data collection, and computation for online surface recognition.

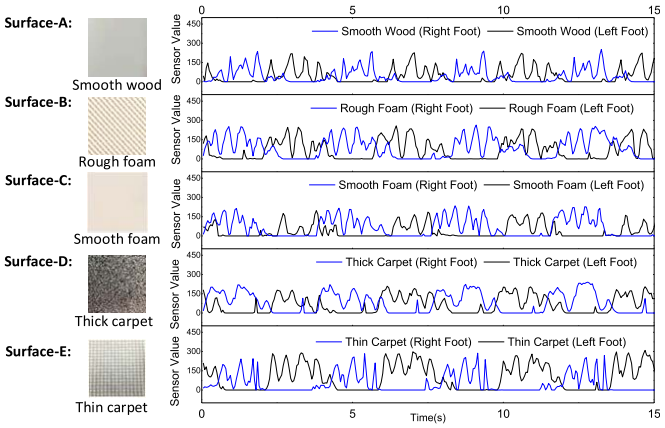

Fig. 4. Raw data from the force sensors mounted under right and left foot of the biped robot, when walking on the 5 kinds of flat surfaces at 190 frames/stride.

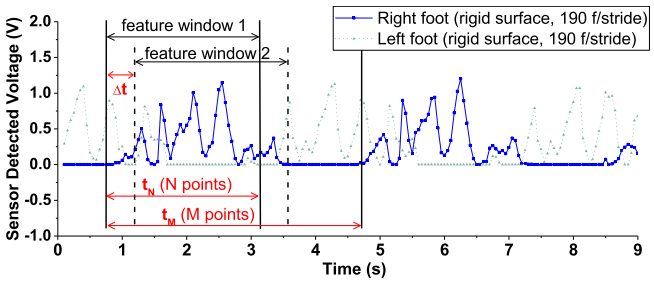

Fig. 5. Overlapped-window-based feature extraction by sliding a N-point feature window of t_N time length in consecutive steps of Δt length over the raw force-sensor data.

C. Data Collection

One critical task for investigating the surface-recognition performance, based on the physical interaction of robot feet and the ground surface, is the surface selection. As illustrated in Fig. 4, five representative types of flat indoor surfaces, listed below, were tested in our experiments.

- Surface-A: smooth wood surface
- Surface-B: rough foam surface
- Surface-C: smooth foam surface
- Surface-D: thick carpet surface
- Surface-E: thin carpet surface

We collected the time series of data streams $D_{force}(i)$ of both feet by a program that is designed and loaded by the Computational Control System (CCS) while the biped robot was walking on the aforementioned five types of surfaces, respectively. M sequential data points of $D_{force}(i)$, sampled from each force sensor at a frequency of $f_{samp} = 20$Hz, were grouped into measurement samples for one stride of the biped robot. Consequently, the total time of a stride of the biped robot can be calculated according to: $T_{stride} = M/f_{samp}$.

Since the surface properties (e.g., rigidity, softness, smoothness, etc.) lead to characteristic changes in the voltage values from the force sensors, surfaces can be distinguished by the differences in the voltage-waveform characteristics of the walking patterns.

D. Overlapped-Window-Based Feature Extraction

To reduce noise interference and improve the classification accuracy, raw force-sensor signals are mapped into higher-dimensional feature vectors, which describe the physical interaction between robot feet and surface more efficiently before the recognition processing. A stepwise segmentation is operated on the time stream of input sensor data, which uses the overlapped windowing technique. The streamed sensor data are sampled by sliding a feature window of N ($0 < N < M$) sensor-data points in size with consecutive steps of a custom-length interval $\Delta t (0 < \Delta t < t_M)$, as illustrated in Fig. 5. The overlapping windows bring more information for pattern identification, when compared to the adjacent-window-based approach (i.e., $N = M$ and $\Delta t = tN = tM$) [39]. The dynamic streaming-feature spaces are created by descriptors from the dynamic time-series raw-sensor data inside an overlapped feature window that moves in steps Δt over time. The processing procedure of feature extraction is equivalent to a convolution between the raw-sensor data and the sliding N-point window. The four kinds of feature descriptors, i.e., RMS, IAV, VAR, and MA, were investigated and compared in our implementation.

E. OVO-Based Multi-Class Recognition Architecture

We employed an improved OVO approach, implemented on the microprocessor ATmega328P, for solving the multi-class classification problem during online surface recognition. The improved OVO approach was estimated with respect to two aspects.

Firstly, the multi-class SVM approach was independently operated with each individual feature descriptor. The trained model for multi-class recognition is represented by a set of parameters $\{(\boldsymbol{\omega}_1, b_1), \ldots, (\boldsymbol{\omega}_{m(m-1)/2}, b_{m(m-1)/2})\}$ where $\boldsymbol{\omega_i} = (\omega_i[1]; \omega_i[2]; \ldots; \omega_i[d])$ is the d-dimensional vector for the i-th binary SVM classifier, $i = 1, 2, \ldots, m(m-1)/2$, while m is the number of possible walking surfaces. Dimensionality d of the weight vector $\boldsymbol{\omega_i}$ is the same as that of the employed feature vectors. The $m(m-1)/2$ pairs of trained model parameters are respectively sent to the parallel SVM classification module for online parallel recognition, as illustrated in Fig. 6. Raw sensor data {x(1), x(2), …, x(N)}, grouped into the N-point windows, are used to calculated the d-dimensional feature vectors $(f(1), f(2), \ldots, f(d))$ by one of the four aforementioned descriptors. For each binary SVM classifier, the sequential components of the dynamic feature vectors are multiplied by the corresponding dimensional component of the trained weight vector. The summation of the multiplications, accumulated by an adder tree, is further added up with the bias to obtain the separating hyperplane of the two different classes. Specifically, the OVO strategy for a multi-class recognition task, using an individual feature descriptor, has to be modified according to the number of possible surfaces. For identifying the $m = 5$ surfaces, ten binary classifiers should be combined to solve the multi-class recognition problem. The possible votes for one class are within the range of [0, 4] as there are four paired binary SVM classifiers related to the same surface for a total of five surfaces. Although there is only one maximum value in most cases, two and more identical

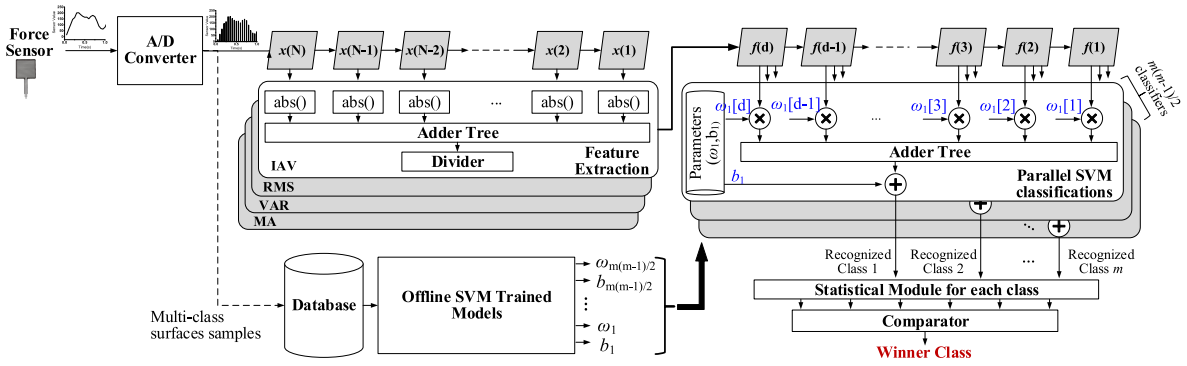

Fig. 6. Overall architecture for online multi-class surface recognition based on the extended OVO voting strategy.

maximum vote values are possible. For example, the votes for each surface {surface-A, surface-B, surface-C, surface-D, surface-E} can lead to {3, 3, 3, 1, 0}, {3, 3, 2, 2, 0}, {3, 3, 2, 1, 1}, or {2, 2, 2, 2, 2} configurations.

Secondly, all feature descriptors are combined for winner-surface voting to further improve the classification performance. The basic implementation architecture is the same as for the first OVO voting strategy, operating with individual feature descriptors. The main change is the simultaneous classification-result evaluation of all $m(m-1)/2{*}4$ binary SVM models with the four feature descriptors by the statistical module in Fig. 6. This means, the classification decision is made by a majority vote from these $m(m-1)/2{*}4$ binary SVM classifiers, based on the above described OVO strategy for multi-class recognition with a single feature descriptor. Since four feature descriptors are now used simultaneously, the range of the possible winner votes for one class changes to [0, 16].

In case of 2 maxima in the above two solutions, the winner class was determined by the direct binary classification results between the two involved surfaces. For more than 2 identical maximum votes the class with a smallest index was picked as the winner.

IV. Experimental Results and Analysis

To evaluate the surface-recognition performance on different indoor-floor surfaces by identifying the walking patterns of the biped robot, we performed a k-fold Cross Validation (CV) in our experiments to investigate the proposed recognition approach, using the improved multi-class SVM classifiers based on the OVO strategy.

Cross validation is an effective and reliable resampling technique for testing the model performance by computing the average of the validation results observed in k iterations. In our experiments, the five representative flat-floor indoor surfaces, described in Section III.C, were investigated. Force-sensory data of 250 robot strides per surface at 190 frames/stride walking speed, were collected for estimating the classification performance of the proposed SVM models using 10-fold CV.

In 10-fold CV, the force sensory dataset was split into 10 independent subsets of equal size. The proposed SVM model was trained for 10 times, each time using 9 of the 10 subsets for training while using the remaining one subset to compute the outcomes of the model evaluations, e.g., accuracy, precision, and recall. The average of the testing outcomes, observed in the 10 iterations, is then reported as the 10-fold CV estimate.

A. Dynamical Feature Extraction

We operated dynamical feature extraction on the raw force sensory data before estimating the recognition performance of the SVM architecture illustrated in Fig.6. To reduce the noise interference and improve the classification accuracy, the SVM classification was based on the dynamical feature vectors, computed by the descriptors as defined in Section II.B and applied the overlapped-window-based strategy as described in Section III.D, rather than on the raw-force data.

Specifically, the raw force-sensory data during robot walking were sampled and segmented into a sequence of robot strides. Each stride is represented by M = 76 data points, which results from the sampling rate of 50 ms/point and the walking speed of 190 frames/stride. For extracting the feature vectors, a feature-window size of N = M/2 points, i.e., N = 38, was applied to slide over the force-sensory data stream in a stepwise manner according to the overlapped-window-based scheme. Further, a sliding step of 1 point (i.e., Δt = 50 ms) between two adjacent feature windows was chosen, as explained in Fig. 5.

The feature-vector dimensionality of one stride in each feature space is supposed to be equivalent to N+M−1, which results from the convolution operation for feature extraction using N-point feature windows and M points of sensor data per stride. However, the obtained streaming curves for the four features remain to have an M-point period. In other words, the dynamic feature vectors, calculated continuously for online pattern recognition, resulted in the same dimension "M" as for each robot stride. Figure 7 illustrates the separate characteristics of the four time-domain feature spaces using RMS, VAR, IAV, and MA, respectively, when the robot walks on the five different surfaces. The different characteristics of these surface-specific waveforms in the four feature spaces, due to the physical-interaction impact, are applied for identifying the corresponding surface. The impact of the waveform differences in each feature space on recognition efficiency is analyzed in the following sections.

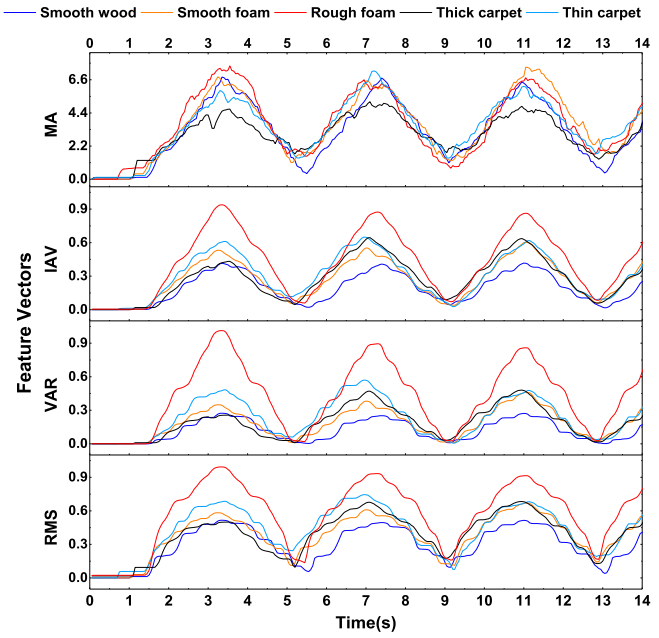

Fig. 7. Normalized four dynamic-feature streams (left foot) as calculated by RMS, VAR, IAV, and MA descriptors, respectively, on 5 different surfaces at 190 frames/stride walking speed.

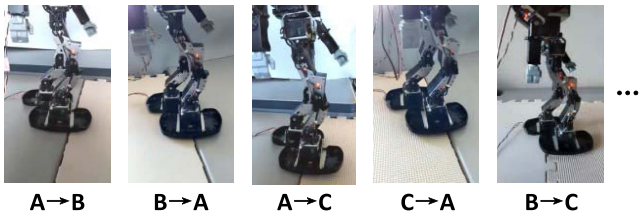

Fig. 8. Examples for illustrating the robot transition between two surfaces. Here, surface A indicates the smooth wood, B refers to the smooth foam, and C represents the rough foam.

B. Binary SVM-Classification Performance

Considering the biped-robot transition between two surfaces, we evaluated the binary classification performance for all two-surface pairs of the five investigated surfaces listed in Section III.C. Figure 8 shows several real scenarios of robot transition across two surfaces.

To verify the recognition performance for all 10 possible pairs between the five investigated surfaces, we constructed the respective binary SVM classifiers, and estimated their performance in terms of precision, recall and accuracy, respectively. To train each binary SVM classification model, 225 samples per surface (i.e., 9 of the 10 folds) were used, and then the trained model was applied to the 25 samples of the remaining fold. This process was iterated for all 10 possibilities of the remaining fold to obtain the 10-fold CV estimate.

The best average precision of the 10-fold CV with our binary SVM classifications reached 100% for distinguishing the thin-carpet surface (i.e., surface-E) from the thick-carpet surface (i.e., surface-D) with all optional feature descriptors. Besides, the average precision for distinguishing the smooth-wood surface (i.e., surface-A) from the thin-carpet surface (i.e., surface-E) was also 100% when employing RMS, IAV or VAR, while 98.8% average precision were achieved

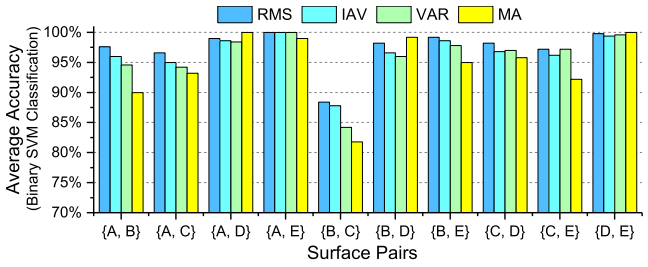

Fig. 9. Average accuracies of the 10-fold cross validation with the ten possible binary SVM classifiers for the four individual feature descriptors, i.e., RMS, IAV, VAR, and MA, with respect to all pairs of the five investigated surfaces mentioned in Section III.C.

with MA. By contrast, the worst average precision with 10-fold CV (RMS: 85.0%, IAV: 84.9%, VAR: 82.0%, MA: 78.9%) happened for distinguishing the rough-foam surface (i.e., surface-B) from the smooth-foam surface (i.e., surface-C).

The best average recall with 10-fold CV reached 100% for distinguishing surface-A from surface-E by employing RMS, IAV or VAR, and for distinguishing surface-D from surface-A and surface-E by employing MA. Approximately 99.2% of average recall rate was achieved with MA for paired surfaces {A, E}. Similarly, the worst average recall with 10-fold CV happened for distinguishing the paired surfaces {B, C}, i.e., RMS: 93.2%, IAV: 92.0%, VAR: 87.6%, MA: 86.8%.

To summarize the impact of our precision and recall analysis, we calculated the average accuracies of each pair of surfaces, using the binary SVM classifications, as illustrated in Fig. 9. For the paired surfaces {A, E}, the best binary accuracies were obtained as RMS: 100%, IAV: 100%, VAR: 100%, MA: 99.0%. Likewise, the worst case of the binary accuracies (RMS: 88.4%, IAV: 87.8%, VAR: 84.2%, MA: 81.8%) happened for distinguishing of the paired surfaces {B, C}. The results for the four feature descriptors reveal, that the best binary-classification performance in terms of average accuracy is reached with the RMS descriptor.

C. Multi-Class SVM Classification With Individual Features

Binary classification is a one-surface versus another-surface scheme, but a one-surface versus all-other-surfaces scheme, which requires multi-class surface recognition, is essential for practical applications of an intelligent biped robot in the human living environment. To estimate the recognition performance of the implemented architecture for the multi-class SVM recognition, we combined the ten trained binary SVM classification models corresponding to each pair of surfaces as aforementioned for online multi-class recognition, basing on the improved OVO approach. In the 10-fold CV estimate, the average outcomes for 10 iterations of the multi-class SVM classification were computed. We investigated the recognition performance of the parallel SVM architecture, exhibited in Fig. 6, using 25 instances of input robot strides (i.e., testing samples) per surface per iteration.

The recall-rate concept for a given surface, corresponding to the i-th class in our multi-class SVM system, is redefined

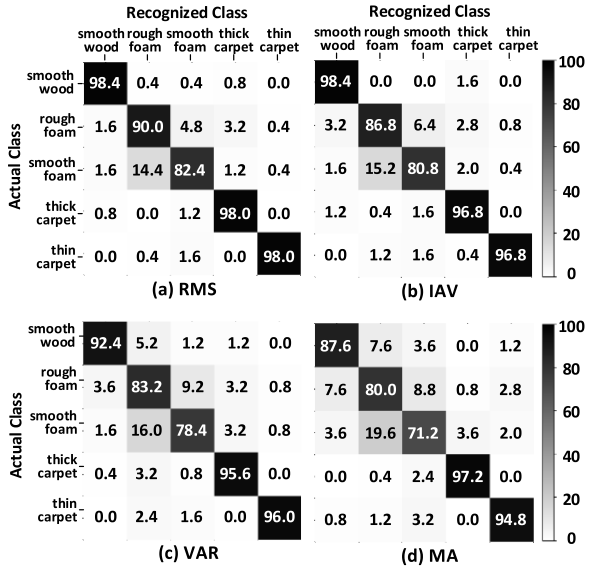

Fig. 10. Confusion matrices of the average recall rates (%), employing the OVO-based strategy for multi-class SVM surface recognition with five different surfaces and a 10-fold CV estimate.

as

$$recall_{mult}(i) = \frac{TP_i}{TP_i + FN_i}. \tag{8}$$

Here, TP_i (i = 1, 2, …, m) is the number of the correctly recognized surface for all testing-surface samples of the i-th class and m ($m = 5$) is the number of surface classes. FN_i is the number of testing-surface samples of the i-th class, which are incorrectly classified into a different class.

The resulting recall rates in each iteration (i.e., fold) of the proposed OVO-based multi-class classification, employing four individual feature descriptors, are listed in Table I.I, Table I.II, Table I.III, and Table I.IV, respectively.

The maximum recall rate according to (8), basing on any one of the four feature descriptors among the 5 surfaces, could achieve 100%. The average recall rates, with 10 folds of the multi-class SVM recognition system for the respective surface, were further computed and summarized in the confusion matrices, as illustrated in Fig. 10. Each row of the confusion matrix gives the average proportional classification distribution for all testing samples of the respective surface with 10-fold CV. The RMS descriptor performed best among the four feature descriptors with respect to the average recall rate of the respective surface, i.e., {98.4%, 90.0%, 82.4%, 98.0%, 98.0%} corresponding to {surface-A, surface-B, surface-C, surface-D, surface-E}, when using the OVO-based multi-class SVM classification strategy.

Likewise, the definition of precision for the i-th class can be expressed within multi-class SVM approach as

$$precision_{mult}(i) = \frac{TP_i}{TP_i + FP_i}, \tag{9}$$

where FP_i is the number of surface-testing samples, incorrectly recognized among all testing samples as belonging to the i-th class. The experimental results of the average precisions, according to (9) with 10 folds of the four feature descriptors for each surface, are summarized in Table II. In particular, for a thin-carpet surface employing the RMS descriptor, a maximum average precision of 99.19% is achieved with our multi-class recognition system.

The overall accuracy of the whole multi-class SVM recognition system is defined as

$$accuracy_{mult} = \frac{\sum_i^m TP_i}{\sum_i^m S(i)} = \frac{1}{m}\sum_i^m p(i,i). \tag{10}$$

Here, S(i) is the total number of all testing-surface samples for all five classes. The overall accuracy can be calculated by the average proportional distribution p(i, i) in the diagonal line at the i-th row and i-th column of the confusion matrices in Fig. 10 as well, when measuring the same number of testing samples for each surface. Therefore, the overall accuracies of our multi-class SVM recognition system resulted in 93.36%, 91.92%, 89.12%, and 86.16%, concerning the four feature descriptors RMS, IAV, VAR, and MA, respectively.

D. Multi-Class SVM Classification With Combined Features

To further improve the classification performance of the multi-class recognition system, we combined the four independent multi-class SVM classifiers, which used one of the four individual feature descriptors, into a single multi-class SVM classifier. In other words, the winner surface is not determined by voting individually, basing on one independent feature descriptor, but results from the voting outcome using all four feature descriptors. Thus, the vote for each surface type is given by the summation of the classification results from all $m(m-1)/2$*4 binary SVM classifiers, based on the four feature descriptors and m surface classes ($m = 5$ in our investigation). The winner surface is determined by these combined votes, based on the "max-win" strategy. Additionally, the surface with a smaller index is selected as the winner in the case of two or more identical maximum votes in this section.

In the 10-fold CV estimate of the combined-feature strategy, we achieved a best recall rate of 100% for at least one of the 10 folds in the case of all five individual surfaces. However, for average recall rates, they were just slightly improved, as illustrated in Fig. 11, in comparison to the four individual-feature-based multi-class SVM classifiers. Namely, recall rates of 98.8% for smooth wood, 91.6% for rough foam, 82.0% for smooth foam, 98.0% for thick carpet, and 98.0% for thin carpet were verified for the combined classifier, as exhibited by the diagonal values of the confusion matrix. The individual precisions for each surface are listed in Table III. A mean average precision of 93.8% was achieved with the combined multi-class classifier. The overall accuracy for the combined classifier resulted in 93.7%, according to the integration over all binary SVM classifiers of the four different descriptors in (10).

E. Comparison With the State-of-the-Arts

In this section, we present diversified types of surface-recognition approaches for various robots, which have

TABLE I
RECALL RESULTS FOR EACH INDIVIDUAL FOLD WITH FOUR INDIVIDUAL FEATURES. (I) RMS FEATURE, (II) IAV FEATURE, (III) VAR FEATURE (IV) MA FEATURE

TABLE I. I RMS FEATURE

Fold index	Recall (%) of each surface using multi-class SVM classification with 10-fold cross validation by RMS feature				
	Smooth wood	Rough foam	Smooth foam	Thick carpet	Thin carpet
1	92.0	88.0	100	92.0	100
2	100	96.0	80.0	100	100
3	100	92.0	96.0	96.0	100
4	100	88.0	12.0	96.0	92.0
5	100	96.0	96.0	96.0	100
6	100	92.0	96.0	100	100
7	100	96.0	100	100	100
8	96.0	72.0	92.0	100	96.0
9	96.0	88.0	76.0	100	92.0
10	100	92.0	76.0	100	100
Max	**100**	**96.0**	**100**	**100**	**100**
Avg	**98.4**	**90.0**	**82.4**	**98.0**	**98.0**

TABLE I. II IAV FEATURE

Fold index	Recall (%) of each surface using multi-class SVM classification with 10-fold cross validation by IAV feature				
	Smooth wood	Rough foam	Smooth foam	Thick carpet	Thin carpet
1	92.0	96.0	96.0	92.0	100
2	100	92.0	92.0	100	100
3	100	92.0	96.0	96.0	100
4	100	84.0	12.0	88.0	96.0
5	100	96.0	96.0	92.0	100
6	100	88.0	100	100	100
7	100	88.0	100	100	100
8	92.0	60.0	80.0	100	88.0
9	100	84.0	60.0	100	84.0
10	100	88.0	76.0	100	100
Max	**100**	**96.0**	**100**	**100**	**100**
Avg	**98.4**	**86.8**	**80.8**	**96.8**	**96.8**

TABLE I. III VAR FEATURE

Fold index	Recall (%) of each surface using multi-class SVM classification with 10-fold cross validation by VAR feature				
	Smooth wood	Rough foam	Smooth foam	Thick carpet	Thin carpet
1	88.0	72.0	96.0	80.0	96.0
2	92.0	96.0	80.0	100	100
3	100	88.0	92.0	96.0	100
4	96.0	84.0	8.0	96.0	92.0
5	100	88.0	88.0	92.0	100
6	88.0	88.0	88.0	100	100
7	96.0	92.0	100	96.0	100
8	84.0	68.0	92.0	96.0	84.0
9	92.0	72.0	68.0	100	88.0
10	88.0	84.0	72.0	100	100
Max	**100**	**96.0**	**100**	**100**	**100**
Avg	**92.4**	**83.2**	**78.4**	**95.6**	**96.0**

TABLE I. IV MA FEATURE

Fold index	Recall (%) of each surface using multi-class SVM classification with 10-fold cross validation by MA feature				
	Smooth wood	Rough foam	Smooth foam	Thick carpet	Thin carpet
1	84.0	76.0	92.0	92.0	96.0
2	92.0	72.0	60.0	100	88.0
3	88.0	84.0	84.0	100	100
4	76.0	72.0	4.0	100	92.0
5	92.0	88.0	96.0	100	96.0
6	88.0	80.0	96.0	100	92.0
7	96.0	96.0	100	96.0	100
8	84.0	76.0	72.0	84.0	92.0
9	84.0	80.0	60.0	100	92.0
10	92.0	76.0	48.0	100	100
Max	**96.0**	**96.0**	**100**	**100**	**100**
Avg	**87.6**	**80.0**	**71.2**	**97.2**	**94.8**

TABLE IV
COMPARISON WITH OTHER STATE-OF-THE-ART WORKS

Schemes	Types of Robots	Sensors	Surface Types	Recognition Algorithms	Control System	Processing Speed	Best Performance
[8]	AMOS II hexapod	Vision	8 outdoor	SIFT/SURF+SVM	Mini-PC with Intel Atom processor	Frame rate < 30 fps (image size=720p)	90.00% (accuracy)
[9]	PhantomX hexapod	Acoustics	7 outdoor	FFT (spectral, band) +SVM	HARK-ROS + Hark designer [40]	N/A	95.1% (sensitivity)
[16]	Developed four-wheeled	Vision & accelerometer	6 outdoor	11 types (e.g. DFT) + Laplacian SVM	Smart phone via Bluetooth	N/A	90.95% (accuracy in TD*); 93.3% (accuracy in FD*)
[20]	SAIL-R hexapod	Capacitive tactile sensors & IMU	8 outdoor	2 Feature sets + SVM	ARM Cortex-M4F microprocessor	41/50ms FE* + prediction time	82.5% (accuracy)
[25]	Sony AIBO quadruped	Infrared range/force & accelerometer	6 indoor	FFT+ RF	MIPS CPU in AIBO	(3.5ms FE * + 20~90 µs prediction) /surface	94% (accuracy)
[30]	WALK-MAN biped	Force/torque & IMU	5 indoor	FFT & DWT + SVM	Torso position compliance controller	N/A	95.16±0.80%(mean precision) 95.0%±0.82 % (mean recall)
[32]	Kondo KHR-3HV biped	Force	5 indoor	Combined features + kNN	ATmega328P + RCB-4HV	(0.708 + 0.028×n)* ms/stride	90.4% (accuracy) 91.5% (precision)
This work	Kondo KHR-3HV biped	Force	5 indoor	Combined features + Combined SVMs	ATmega328P + RCB-4HV	0.73 ms/stride	93.7% (mean accuracy) 93.8% (mean precision)

*TD: Time Domain; FD: Frequency Domain; FE: Feature Extraction; n = number of reference samples (n≥2)

been developed for different applications in recent years and compare their classification performances with our results in Table IV. The vision-based recognition solution [8] achieved 90% accuracy for eight surfaces, but normally asks for much more computational resources and computing time for image processing. Christie *et al.*, [9] proposed an acoustics-based terrain-classification solution with an OVO-based multi-class SVM classifier and obtained up to 95.1% sensitivity (i.e., recall) with nose removal for hexapod robots, employing FFT to extract spectral features and band features from the acoustic information of each gait cycle. This increased the sensing diversity for a more versatile solution of surface recognition.

TABLE II
COMPARISON OF 10-FOLD AVERAGE PRECISION FOR MULTI-CLASS SVM CLASSIFICATION

Feature Descriptors	Precision (%) of each surface using multi-class SVM				
	Smooth wood	Rough foam	Smooth foam	Thick carpet	Thin carpet
RMS	96.09	91.15	85.55	94.96	99.19
IAV	94.25	89.38	83.78	93.44	98.78
VAR	94.29	85.96	75.64	92.64	98.36
MA	87.95	79.82	73.53	95.67	94.05

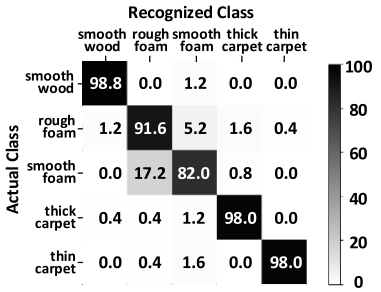

Fig. 11. Confusion matrix the average recall rates (%) for the 5 investigated surfaces, obtained with the OVO-based multi-class SVM classification and the combination of the RMA, IAV, VAR, and MA feature descriptors.

TABLE III
PRECISION OF COMBINED MULTI-CLASS SVM CLASSIFIER

Feature Descriptors	Average precision (%) of each surface, using the combined classifier with 10-fold CV				
	Smooth wood	Rough foam	Smooth foam	Thick carpet	Thin carpet
Combined Features	98.4	83.6	89.9	97.6	99.6

Shi *et al.*, [16] reported a modified Laplacian SVM solution of terrain classification for a four-wheeled mobile robot, based on a vision sensor and an accelerometer, which achieved 90.95% total classification accuracy using time-domain features and 93.3% accuracy using frequency-domain features. Wu *et al.*, [20] navigated hexapod the robot using capacitive tactile sensors and an IMU, resulting in 82.5% overall accuracy for recognizing eight surfaces by the SVM classifier. Kertész [25] applied the FFT magnitude over the data from four fused sensors for feature vectors and analyzed the machine learning aspects with random forests (RFs), thus achieving 94% accuracy when distinguishing six types of indoor surfaces for a quadruped robot. A fusion scheme of multiple sensors collects more useful information for higher classification accuracy, but it requires more complex computation. Besides, surface recognition based on a single sensor type resulted in poor accuracy performance, such as 48.1% using an accelerometer or 62.7% using ground contact force sensors [25]. Walas *et al.* [30] used the FFT and DWT to produce feature vectors and performed a learning procedure using SVM in two approaches. The best performance in [30] led to 91.01±1.94% "mean precision" and 90.7%±1.94% "mean recall" for the FFT approach. 95.16±0.80% "mean precision" and 95.0%±0.82 % "mean recall" were achieved for DWT approach. Our previous work employed kNN [32] as classifier and achieved slightly lower overall accuracy and average precision. Moreover, kNN requested more resources for storing the references and resulted in longer computational times. Note that the feature-descriptor combination in this work is different from the OVA (One-Versus-All)-based form in [32]. We fused all feature vectors produced from the four feature descriptors together for direct winner-surface voting in the combined multi-class SVM classifier. Besides, >10% binary-accuracy improvement is achieved for each feature descriptor using the SVM classifier, as compared to the kNN classifier in [32]. The required computational times of the applied schemes of the previous works, listed in Table IV, which are equipped with different control systems, are further influenced by the employed disparate measurements. Nevertheless, the processing speed of 0.73 ms/stride in this work is very competitive for real-time applications, according to the analysis in Table IV.

V. CONCLUSION

In this work, we investigated the surface-recognition performance for five indoor surfaces with different properties via walking-pattern classification of a biped robot KHR-3HV, based on cost-economic membrane force sensors, to ensure a safe transition between different surfaces. To achieve robust recognition results with an efficient hardware implementation, the online surface-recognition system was implemented on an RCB-4HV controller and a low-cost Arduino UNO board. An overlapped-window-based feature-extraction method was used for producing feature vectors from the dynamical force-sensory data stream, applying four time-domain feature descriptors, namely, MA, IAV, VAR, and RMS. Given the multi-class recognition problem, 10 binary SVMs for each individual feature descriptor were combined for multi-class walking-pattern classification based on an extended OVO strategy. Four feature descriptors were further fused with respect to the winner-surface voting, achieving recall rates of 98.8%, 91.6%, 82.0%, 98.0%, 98.0% for smooth wood, rough foam, smooth foam, thick carpet, and thin carpet, respectively. Additionally, 93.8% mean average precision and 93.7% average accuracy were obtained in this 10-fold cross validation. The experimental results of this work show, that our cost-economic approach can be useful for achieving robust surface recognition and ensuring safe locomotion for biped robots.

VI. FUTURE WORK

To better understand the human living environment and to make the biped robot more intelligent in supporting human beings, we plan in the future to employ several force sensors beneath its feet. A concept extension to the increased feet number of multi-legged robots is also promising. Besides, more cost-efficient force sensing techniques such as the sensing blankets are feasible for other robot types, like wheeled robots. The use of various other sensors, like image sensors,

for increasing the robot's sensing diversity also belongs to our future plan, thus achieving further increased stability and recognition accuracy by combining an abundance sensory data.

REFERENCES

[1] J. Denny, M. Elyas, S. A. D'Costa, and R. D. D'Souza, "Humanoid robots-past, present and the future," *Eur. J. Adv. Eng. Techni.*, vol. 3, no. 5, pp. 8–15, 2016.

[2] Y. H. Yin, Y. Xu, Z. H. Jiang, and Q. R. Wang, "Tracking and understanding unknown surface with high speed by force sensing and control for robot," *IEEE Sensors J.*, vol. 12, no. 9, pp. 2910–2916, Sep. 2012.

[3] V. B. Semwal, A. Bhushan, and G. C. Nandi, "Study of humanoid push recovery based on experiments," in *Proc. Int. Conf. Control, Autom., Robot. Embedded Syst. (CARE)*, Jabalpur, India, Dec. 2013, pp. 1–6.

[4] V. B. Semwal, S. A. Katiyar, R. Chakraborty, and G. C. Nandi, "Biologically-inspired push recovery capable bipedal locomotion modeling through hybrid automata," *Robot. Auto. Syst.*, vol. 70, pp. 181–190, Aug. 2015.

[5] V. B. Semwal and G. C. Nandi, "Generation of joint trajectories using hybrid automate-based model: A rocking block-based approach," *IEEE Sensors J.*, vol. 16, no. 14, pp. 5805–5816, Jul. 2016.

[6] V. B. Semwal, C. Kumar, P. K. Mishra, and G. C. Nandi, "Design of vector field for different subphases of gait and regeneration of gait pattern," *IEEE Trans. Autom. Sci. Eng.*, vol. 15, no. 1, pp. 104–110, Jan. 2018.

[7] Y. N. Khan, P. Komma, and A. Zell, "High resolution visual terrain classification for outdoor robots," in *Proc. IEEE Int. Conf. Comput. Vis. Workshops (ICCV Workshops)*, Barcelona, Spain, Nov. 2011, pp. 1014–1021.

[8] S. Zenker, E. E. Aksoy, D. Goldschmidt, F. Worgotter, and P. Manoonpong, "Visual terrain classification for selecting energy efficient gaits of a hexapod robot," in *Proc. IEEE/ASME Int. Conf. Adv. Intell. Mechatronics*, Wollongong, NSW, Australia, Jul. 2013, pp. 577–584.

[9] J. Christie and N. Kottege, "Acoustics based terrain classification for legged robots," in *Proc. IEEE Int. Conf. Robot. Autom. (ICRA)*, Stockholm, Sweden, May 2016, pp. 3596–3603.

[10] A. Valada, L. Spinello, and W. Burgard, "Deep feature learning for acoustics-based terrain classification," *Robot. Res.*, vol. 3, pp. 21–37, Jul. 2017.

[11] K. Walas and M. Nowicki, "Terrain classification using laser range finder," in *Proc. IEEE/RSJ Int. Conf. Intell. Robots Syst.*, Chicago, IL, USA, Sep. 2014, pp. 5003–5009.

[12] E. M. DuPont, C. A. Moore, E. G. Collins, and E. Coyle, "Frequency response method for terrain classification in autonomous ground vehicles," *Auto. Robots*, vol. 24, no. 4, pp. 337–347, Jan. 2008.

[13] S. Khaleghian and S. Taheri, "Terrain classification using intelligent tire," *J. Terramechanics*, vol. 71, pp. 15–24, Jun. 2017.

[14] A. Vicente, J. Liu, and G.-Z. Yang, "Surface classification based on vibration on omni-wheel mobile base," in *Proc. IEEE/RSJ Int. Conf. Intell. Robots Syst. (IROS)*, Hamburg, Germany, Sep. 2015, pp. 916–921.

[15] C. Bai, J. Guo, and H. Zheng, "Three-dimensional vibration-based terrain classification for mobile robots," *IEEE Access*, vol. 7, pp. 63485–63492, May 2019.

[16] W. Shi, Z. Li, W. Lv, Y. Wu, J. Chang, and X. Li, "Laplacian support vector machine for vibration-based robotic terrain classification," *Electronics*, vol. 9, no. 3, p. 513, Mar. 2020.

[17] W. Lv, Y. Kang, W. Xing Zheng, Y. Wu, and Z. Li, "Feature-temporal semi-supervised extreme learning machine for robotic terrain classification," *IEEE Trans. Circuits Syst. II, Exp. Briefs*, vol. 67, no. 12, pp. 3567–3571, Dec. 2020, doi: 10.1109/TCSII.2020.2990661.

[18] J. J. Shill, E. G. Collins, Jr., E. Coyle, and J. Clark, "Tactile surface classification for limbed robots using a pressure sensitive robot skin," *Bioinspiration Biomimetics*, vol. 10, no. 1, Feb. 2015, Art. no. 016012.

[19] V. A. Ho, M. Makikawa, and S. Hirai, "Flexible fabric sensor toward a humanoid Robot's skin: Fabrication, characterization, and perceptions," *IEEE Sensors J.*, vol. 13, no. 10, pp. 4065–4080, Oct. 2013.

[20] X. A. Wu, T. M. Huh, A. Sabin, S. A. Suresh, and M. R. Cutkosky, "Tactile sensing and terrain-based gait control for small legged robots," *IEEE Trans. Robot.*, vol. 36, no. 1, pp. 15–27, Feb. 2020.

[21] K. Walas, "Terrain classification and negotiation with a walking robot," *J. Intell. Robotic Syst.*, vol. 78, nos. 3–4, pp. 401–423, Jun. 2015.

[22] J. Mrva and J. Faigl, "Feature extraction for terrain classification with crawling robots," in *Proc. ITAT*, Prague, Czech Republic, 2015, pp. 179–185.

[23] M. A. Hoepflinger, C. D. Remy, M. Hutter, L. Spinello, and R. Siegwart, "Haptic terrain classification for legged robots," in *Proc. IEEE Int. Conf. Robot. Autom.*, Anchorage, AK, USA, May 2010, pp. 2828–2833.

[24] C. Kertesz, "Exploring surface detection for a quadruped robot in households," in *Proc. IEEE Int. Conf. Auto. Robot Syst. Competitions (ICARSC)*, Espinho, Portugal, May 2014, pp. 152–157.

[25] C. Kertesz, "Rigidity-based surface recognition for a domestic legged robot," *IEEE Robot. Autom. Lett.*, vol. 1, no. 1, pp. 309–315, Jan. 2016.

[26] X. Li, W. Wang, and J. Yi, "Ground substrate classification for adaptive quadruped locomotion," in *Proc. IEEE Int. Conf. Robot. Autom. (ICRA)*, Singapore, May 2017, pp. 3237–3243.

[27] R. Matsumura, M. Shiomi, T. Miyashita, H. Ishiguro, and N. Hagita, "What kind of floor am i standing on? Floor surface identification by a small humanoid robot through full-body motions," *Adv. Robot.*, vol. 29, no. 7, pp. 469–480, Apr. 2015, doi: 10.1080/01691864.2014.996601.

[28] F. Asano, H. Asoh, M. Morisawa, S. Kajita, and K. Yokoi, "Risk evaluation of ground surface using multichannel foot sensors for biped robots," in *Proc. IEEE Int. Symp. Robotic Sensors Environ. (ROSE)*, Timişoara, Romania, Oct. 2014, pp. 61–65.

[29] L. Almeida, V. Santos, and J. Ferreira, "Learning-based analysis of a new wearable 3D force system data to classify the underlying surface of a walking robot," *Int. J. Hum. Robot.*, vol. 17, no. 3, Jun. 2020, Art. no. 2050011, doi: 10.1142/.S0219843620500115.

[30] K. Walas, D. Kanoulas, and P. Kryczka, "Terrain classification and locomotion parameters adaptation for humanoid robots using force/torque sensing," in *Proc. IEEE-RAS 16th Int. Conf. Humanoid Robots (Humanoids)*, Cancún, Mexico, Nov. 2016, pp. 133–140.

[31] J. M. Gandarias, A. J. Garcia-Cerezo, and J. M. Gomez-de-Gabriel, "CNN-based methods for object recognition with high-resolution tactile sensors," *IEEE Sensors J.*, vol. 19, no. 16, pp. 6872–6882, Aug. 2019.

[32] S. Bhattacharya *et al.*, "Surface-property recognition with force sensors for stable walking of humanoid robot," *IEEE Access*, vol. 7, pp. 146443–146456, Oct. 2019.

[33] A. Luo *et al.*, "Dynamic pattern-recognition-based walking-speed adjustment for stable biped-robot movement under changing surface conditions," in *Proc. IEEE 8th Global Conf. Consum. Electron. (GCCE)*, Osaka, Japan, Oct. 2019, pp. 600–601.

[34] X. Xi, M. Tang, S. M. Miran, and Z. Luo, "Evaluation of feature extraction and recognition for activity monitoring and fall detection based on wearable sEMG sensors," *Sensors*, vol. 17, no. 6, p. 1229, May 2017.

[35] A. C. Turlapaty and B. Gokaraju, "Feature analysis for classification of physical actions using surface EMG data," *IEEE Sensors J.*, vol. 19, no. 24, pp. 12196–12204, Dec. 2019.

[36] B. Hudgins, P. Parker, and R. N. Scott, "A new strategy for multifunction myoelectric control," *IEEE Trans. Biomed. Eng.*, vol. 40, no. 1, pp. 82–94, Jan. 1993.

[37] K. K. Co and L. T. Japan. *Specification of KHR-3HV Version 2 Robot*. Accessed: Dec. 20, 2018. [Online]. Available: https://kondo-robot.com/product/03178

[38] Taiwan Alpha Electronic Co., Taipei, Taiwan. *Specification of Membrane Force Sensors Provided by Alpha*. Accessed: Apr. 10, 2019. [Online]. Available: http://www.taiwanalpha.com/en/products/21

[39] M. Hakonen, H. Piitulainen, and A. Visala, "Current state of digital signal processing in myoelectric interfaces and related applications," *Biomed. Signal Process. Control*, vol. 18, pp. 334–359, Apr. 2015.

[40] K. Nakadai, T. Takahashi, H. G. Okuno, H. Nakajima, Y. Hasegawa, and H. Tsujino, "Design and implementation of robot audition system 'HARK'—Open source software for listening to three simultaneous speakers," *Adv. Robot.*, vol. 24, nos. 5–6, pp. 739–761, Jan. 2010.

Aiwen Luo (Member, IEEE) received the B.Eng. degree from Beijing Jiaotong University in 2009, and the M.Eng. degree from Jinan University, China, in 2012, and the D.Eng. degree from Hiroshima University, Japan, in March 2018. From April 2018 to August 2019, she worked as a Postdoctoral Researcher with Hiroshima University. She currently works with Jinan University, the University of Macau, and Hiroshima University. Her research interests include hardware-oriented computer vision, pattern recognition, and intelligent robotics.

Sandip Bhattacharya received the Ph.D. (Eng.) degree from the Indian Institute of Engineering Science and Technology (IIEST), India, in 2017. From October 2017 to December 2020, he worked as a Postdoctoral Researcher with the HiSIM Research Center, Hiroshima University, Japan. He is currently working as an Associate Professor with SR University, Warangal, India. His current research interests include nano device, interconnect modeling, and intelligent circuit design for robotics.

Sunandan Dutta received the M.Tech. degree from the Indian Institute of Engineering Science and Technology (IIEST), Shibpur, India, in 2017. He is currently pursuing the Ph.D. degree with the Graduate School of Engineering, Hiroshima University, Japan. His research interests include the areas of humanoid robotics and system cybernetics.

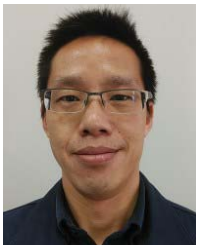

Yoshihiro Ochi received the B.Eng. degree from Tottori University, Tottori, Japan, in 2003. Since 2009, he has been with the Technical Center, Hiroshima University, Higashihiroshima, Japan, where he is also involved in technical support of the information system.

Mitiko Miura-Mattausch (Fellow, IEEE) received the D.Sc. degree from Hiroshima University, Japan. She has been a Professor with Hiroshima University since 1996, where she is also leading the Ultra-scaled Device Laboratory.

Jian Weng (Member, IEEE) received the B.S. and M.S. degrees in computer science and engineering from the South China University of Technology, in 2000 and 2004, respectively, and the Ph.D. degree in computer science and engineering from Shanghai Jiao Tong University, in 2008. From 2008 to 2010, he held a Postdoctoral position at the School of Information Systems, Singapore Management University. He is currently a Professor, the Dean of the College of Information Science and Technology, and the Vice-Chancellor of Jinan University. His research interests include public key cryptography, cloud security, blockchain, and artificial intelligence. He served as the PC Co-Chairs or a PC member for more than 30 international conferences. He serves as an Associate Editor for the IEEE TRANSACTIONS ON VEHICULAR TECHNOLOGY.

Yicong Zhou (Senior Member, IEEE) received the B.S. degree from Hunan University, Changsha, China, and the M.S. and Ph.D. degrees from Tufts University, Medford, MA, USA, all in electrical engineering. He is currently an Associate Professor and the Director of the Vision and Image Processing Laboratory, Department of Computer and Information Science, University of Macau. His research interests include image processing, computer vision, machine learning, and multimedia security. He is a Senior Member of the International Society for Optical Engineering (SPIE). He was a recipient of the Third Price of Macao Natural Science Award in 2014 and 2020. He is the Co-Chair of Technical Committee on Cognitive Computing in the IEEE Systems, Man, and Cybernetics Society. He serves as an Associate Editor for IEEE TRANSACTIONS ON NEUTRAL NETWORKS AND LEARNING SYSTEMS, IEEE TRANSACTIONS ON CIRCUITS AND SYSTEMS FOR VIDEO TECHNOLOGY, IEEE TRANSACTIONS ON GEOSCIENCE AND REMOTE SENSING, and four other journals.

Hans J. Mattausch (Senior Member, IEEE) received the Ph.D. degree from Stuttgart University, Stuttgart, Germany. He has been a Professor with Hiroshima University, Japan, since 1996, where he is also involved in researching on very large-scale integration design, nano-electronics, and compact modeling.